J Math Chem (2009) 45:981–1003
DOI 10.1007/s10910-008-9395-2

ORIGINAL PAPER

Computing the chemical reaction path with a ray-based fast marching technique for solving the Hamilton-Jacobi equation in a general coordinate system

Bijoy K. Dey · Paul W. Ayers

Received: 25 February 2008 / Accepted: 20 March 2008 / Published online: 14 June 2008

Abstract This article presents a ray-based fast marching approach for solving the static Hamilton-Jacobi equation. The approach is very general and can be used for both orthogonal and non-orthogonal coordinate system. The method is unconditionally stable, algorithmatically simple and highly accurate. As an application, we use the method to compute different types of reaction path. Specifically, we consider the path for which the change in action or time is less than that of all other conceivable paths connecting two states. Such reaction paths are efficiently evaluated by back-tracing on the least-action or least-time surfaces. The method is illustrated by applying it to the collinear reactions, $F + H_2 \rightarrow HF + H$ and $HF + H \rightarrow H + FH$.

Keywords Potential energy surface · Reaction path · Least-action · Least-potential · Least-time · Ray method · Fast marching algorithm

1 Introduction

Chemists are familiar with the description of a chemical reaction as a smooth progression along a reaction path on the potential energy hypersurface connecting reactants with products. Reactants, products and stable intermediates are minima on the hypersurface; the transition state is a saddle point with higher energy than the stable structures. The height of the energy barrier separating reactants from products is related to the overall rate of reaction. The reaction path provides a microscopic atom-by-atom and bond-by-bond description of the progress of the reaction, and minima along the reaction coordinate are associated with equilibrium geometries of reactive intermediates. The relative energies of the reactants and products determine the heat of reac-

B. K. Dey (✉) · P. W. Ayers
Department of Chemistry, McMaster University, 1280 Main St. West, Hamilton, ON, Canada
e-mail: bijoy@scienide.uwaterloo.ca

tion. Although such descriptions are known in the transition state theory, theoretical techniques for predicting the product(s) of chemical reactions and their associated reaction paths are extremely limited, even for systems with few degrees-of-freedom. Needless to say, a general computational framework for predicting the products and the reaction pathways would be extremely useful.

Conventional molecular dynamics (MD) approaches [1] (whether based on classical Hamilton's equation of motion or ab initio Carr-Parrinello type [2] MD simulation) are sometimes impractical for reactions because reactions are rare events, i.e., one reaction event may be separated from the next by a time much longer than the duration of a feasible MD simulation. It is impractical to exhaustively map out an entire potential energy surface, except for very small systems [3]. Methods like Chandler's path sampling [4] allow a statistically sound study of the trajectories connecting two points of the configuration space; however, a sample trajectory must be known.

When direct simulation is impractical, a two-level approach bears consideration. In a two-level approach, one uses a semi-quantitative description of a reacting system to find (approximate) potential intermediates and reaction products. With the key intermediates and reaction products known, one may then characterize potential reaction paths with established techniques [5–7], obtaining accurate information about the chemical reaction's properties. Indeed such methods for characterizing chemical processes have been proposed before [8,9]. In what follows, however, the emphasis is on a general technique, applicable to the widest possible range of chemical phenomena. To this end, and for developing a general technique for studying reaction dynamics, we have previously proposed a method [10,11] based on an efficient solution to the Hamilton-Jacobi equation for the least-action path (and a similar equation for the least-time and least-potential paths [11]). Ideally, in theoretical study of reaction dynamics we start with the knowledge of the reactant state and want to calculate, without relying too much on intuition, the feasible product state(s), the transition state(s), the key intermediates and the pathway(s). In this regards, the fast marching level set method [12–14] and the global solution of the classical static HJ equation [10,11,15], supplemented by a back-tracing method [10], provide a good description of the chemical reaction dynamics.

The method has been formulated in a manner in which one can naturally bypass the time-step, dt, and embrace a spatial-step $d\mathbf{q} = [dq_1, dq_2, \ldots, dq_N]^T$. This is important because the resolution of the characteristic motion of the reactive system can be significantly different for a fixed $d\mathbf{q}$ than that for a fixed dt. For instance, a femtosecond time-step corresponds to an extremely fine spatial resolution of the low frequency modes of the system. A reasonable spatial step for a low frequency motion corresponds to several hundred dt in a standard MD simulation.

Previously, we showed how the fast-marching method could be used to find various classical [10,11,15] and tunneling [16] reaction paths for several reaction systems. Although previous fast marching methods are unconditionally stable, highly efficient and algorithmically simple, they suffer from the following drawbacks. (1) The method is accurate only to first order since it is based on a two-point finite-difference formula for the differential operator in the HJ equation. This low-order approximation can result in relatively large errors in the global solution (such as the minimum action/time/potential), particularly in two cases [17], namely, (a) when there is a large

wavefront curvature, such as near the source; (b) when the wavefront propagation is diagonal to the grid orientation. This low-order approximation FMM scheme also demands very fine grid space. (2) The method can be applied only to an orthogonal coordinate systems [12–14] (e.g., Cartesian coordinate) [10,11,16] (For non-orthogonal coordinate systems a coordinate transformation is needed [11,16]) unless the kinetic energy is unimportant in the dynamics (e.g., for the minimum potential energy path [11]). Although alternative fast marching methods for unstructured grids (triangulated meshes) [18,19], higher-order finite difference formulas [20,21], non-orthogonal coordinate [17,22] systems, and a fast sweeping method [23,24] (FSM) exist in the literature, these methods have greater algorithmic complexity and restrictive applicability. No one has ever implemented these more complex fast marching methods in chemical reaction dynamics.

This paper presents a very general new fast marching method based formulation for solving the HJ equation. This method does not reuire the use of the finite-difference approximations for the derivatives and hence reduces the inaccuracy of the conventional FMM based on finitite-difference approximations; this method can be applied to any coordinate systems without any additional effort as the coordinate system changes; this method is unconditionally stable, highly efficient and algorithmically simple; this method can be applied across a broad range of problems, from image processing, to computer visualization, to several geophysical problems. This method can also be used to find chemical reaction paths which is our primary interest.

The remainder of this paper is organized as follows. In Sect. 2 we describe the method. In this context we briefly discuss the least-action and the least-time paths based on classical mechanics, the HJ equations for the action, time, and potential energy, and existing methods for solving the HJ equation. The algorithmic details of the present method are presented in Sect. 3. Illustrations are made in Sect. 4. Here we compute the paths for the reactions, $F + H_2 \longrightarrow HF + H$ and $H + FH \longrightarrow HF + H$ represented in a non-Cartesian coordinate system. Section 5 concludes the paper.

2 Theoretical development

2.1 Least-action/least-time/least-potential paths

Mathematically, the principle of stationary action [25,26] can be stated in its Lagrangian,

$$\delta \int_{initial}^{final} P \cdot dQ = 0, \tag{1}$$

or Hamiltonian form,

$$\delta \int_{initial}^{final} L dt = 0. \tag{2}$$

Here P and Q are the generalized atomic momentum and position vectors and L the Lagrangian. We may enunciate it as follows: a system moves from one configuration

to another in such a way that the values of the action integral for the path taken and the neighboring virtual paths are the same (to first order). Such virtual paths are either co-terminus in space (same end points) and energy (Lagrange's principle) or co-terminus in space and time (Hamilton's principle). All of these virtual paths are potential paths.

The action can be written (we use mass-weighted coordinates with m = 1) as

$$S = \int 2T\,dt = \int 2(E - V)dt = \int \sqrt{2(E - V)}d\mathbf{s} \tag{3}$$

Substituting potential energy by its average value $\langle V \rangle$ over the interval, we get $S = 2(E - \langle V \rangle)\Delta t$. Thus the minimum action path can correspond to a trajectory that climbs up on the potential energy surface in the direction of the final state minimizing this product. This means that minimum action paths tend to pass through high energy regions of the potential energy surface, because the kinetic energy is smaller there. These high-energy paths are improbable dynamical events. (For small E however, the minimum action paths sometimes represent more likely dynamical events.)

Similarly the time a system spends traversing a path can be written as

$$\tau = \int \frac{d\mathbf{s}}{v} = \left(\int \sqrt{2(E - V)} \right)^{-1} d\mathbf{s} \tag{4}$$

where v is the velocity at any point along the path. The stationary time principle is then given as $\delta\tau = 0$. Clearly, high velocity reduces the transit time and the least-time path tends to avoid molecular configuration with high potential energy. The path a light ray follows (Fermat's principle), and the path of a particle constrained to a curve and under the influence of gravity (Brachistochrone) are two examples of least-time paths. Minimum time paths may represent the more realistic reaction paths since, unlike minimum action paths, they stay in the relatively lower energy region of the PES.

Similarly, defining a function, $\tau^{(n)}$ as [11]

$$\tau^{(n)} = \int \left(\sqrt{2(E - V)} \right)^{n+1} dt = \int \left(\sqrt{2(E - V)} \right)^{n} d\mathbf{s} \tag{5}$$

we see that for large negative value of n, $\tau^{(n)}$ decreases as V decreases. Thus, the path corresponding to minimum $\tau^{(n)}$ is the minimum potential energy path, in other words, minimum $\tau^{(n)}$ paths for $n = -\infty$ tend to follow the lowest energy region of the potential energy surface.

2.2 Hamilton-Jacobi equation

Consider the 3N dimensional vector $\mathbf{X} = (x_1, x_2, \ldots, x_{3N})^T$ vector representing the position of the atomic nuclei in the Cartesian coordinate system. The vectors $\mathbf{Q} = (q_1, \ldots, q_{3N})^T$ and $\mathbf{R} = (R_1, \ldots, R_M)^T$ represent the mass-weighted and the internal coordinate (non-Cartesian) system of the molecule, where $q_i = \sqrt{m_i} x_i$ denotes the mass-weighted position vectors for the nuclei i and M denotes the total number of

internal degrees of freedom. The corresponding momentum vectors are $\mathbf{P}_X, \mathbf{P}_Q$ and $\mathbf{P}_R$ respectively. In order to obtain a general form for the Hamilton Jacobi equation in a general coordinate system we start with the function $\tau^{(n)}$ and the mass-weighted coordinate system. In the end we will transform the equation to curvilinear coordinate system. Thus we have,

$$\begin{aligned}\tau^{(n)}(\mathbf{Q}_0(t_0), \mathbf{Q}_f(t_f)) &= \int_{Q_0}^{Q_f} \left(\sqrt{2T(\mathbf{Q}(t))}\right)^{n+1} dt \\ &= \int_{Q_0}^{Q_f} \left(\sqrt{2(E - V(\mathbf{Q}(t)))}\right)^{n+1} dt \end{aligned} \tag{6}$$

Here the relations $T = 1/2\mathbf{P}_Q^T\mathbf{M}^{-1}\mathbf{P}_Q$ and $\mathbf{P}_Q = \mathbf{M}d\mathbf{Q}/dt$ have been used. $\mathbf{M}$ is the mass matrix. In the above equation V($\mathbf{Q}$) is the potential function and E is the total energy of the system. The time variable in the above equation is not an independent variable since it depends on the path. A rigorous definition of path can be made by parameterizing the curve using the line element $\mathbf{s}(\Theta)$, for the trajectory (Θ denotes the parameterization of the path.) [27,28]. The time it takes for a particle to cross a given point on the curve is related to the velocity, $d\mathbf{s}(\Theta)/dt$ at that point. This gives $2T = (d\mathbf{s}/dt)^2$ [27] and so

$$dt = \frac{|d\mathbf{s}(\Theta)|}{\sqrt{2(E - V(\mathbf{Q}(\Theta)))}} \tag{7}$$

Since $|d\mathbf{s}| = \sqrt{\sum (ds_i)^2}$ and $ds_i = \partial s_i/\partial\Theta d\Theta$ we obtain

$$dt = \frac{|D\mathbf{s}(\Theta)|}{\sqrt{2(E - V(\mathbf{Q}(\Theta)))}} d\Theta \tag{8}$$

where $|D\mathbf{s}(\Theta)| = \sqrt{\sum_i (\partial s_i/\partial\Theta)^2}$ and s_i corresponds to the component of $\mathbf{s}$ along q_i. Equation 7 now can be written as

$$\tau^{(n)}(\mathbf{Q}_0(t_0), \mathbf{Q}_f(t_f)) = \int_{\Theta_0}^{\Theta_f} \frac{|D\mathbf{s}(\Theta)|}{(2(E - V(\mathbf{Q}(\Theta))))^{n/2}} d\Theta \tag{9}$$

One can immediately obtain the differential form for the above integral equation (Eq. 10) (see [29]) (from now on, we simply write $\tau^{(n)}(\mathbf{Q})$ for $\tau^{(n)}(\mathbf{Q}_0(t_0), \mathbf{Q}_f(t_f))$ for a fixed initial configuration).

$$\frac{|\nabla\tau^{(n)}(Q)|}{[2(E - V(Q))]^{n/2}} = 1, \ \ or \ \ \nabla\tau^{(n)}(\mathbf{Q}) \cdot \nabla\tau^{(n)}(\mathbf{Q}) = [2(E - V(\mathbf{Q}))]^n \tag{10}$$

This is a general form for the Hamilton Jacobi equation (eikonal equation) in mass-weighted orthogonal coordinate system. For $n = 1$, we have the classical Hamilton-Jacobi equation and so $\tau^{(1)} = S$ (Eq. 3) is Hamilton's characteristic function (classical

action). For $n = -1$ the function $\tau^{(-1)} = \tau$ (Eq. 4) is the time function. For $n = 0$ the function $\tau^{(0)}$ is the distance function, which can be used to generate geodesic curves. The Hamilton-Jacobi equation is readily generalized to a general coordinate system, denoted by **R**, as

$$(\nabla\tau^{(n)}(\mathbf{R}))^T \mathbf{G}(\nabla\tau^{(n)}(\mathbf{R})) = [2(E - V(\mathbf{R}))]^n, \tag{11}$$

where **G** defines the metric for the transformation from **Q** to **R**, the elements of which are $G_{ij} = \partial R_i/\partial q_j$. In general, **G** depends on the coordinate however, in our examples, the metric **G** is a constant metric. When **G** is a unit matrix we get the orthogonal coordinate system. We propose a general algorithm to solve this Hamilton-Jacobi equation and obtain the least-$\tau^{(n)}$ level curves. The algorithm is described below.

2.3 Solution of HJ Equation: existing method

Using a ray-based fast marching method (see the next section) supplemented by back-tracing as described in the later sections, we solve Eq. 11 for the least-$\tau^{(n)}$ (where the cost is the action, the time or the potential) paths. The HJ equation above describes wave front propagation [14] with the "speed" of the wave front related to $1/[2(E - V)]^n$. (Here the definition of the "speed" is the change in distance for every unit change in the value of $\tau^{(n)}$.) Consider a wave front given as $\Gamma_\tau^{(n)}(a) = \{\mathbf{R} \in R^N; \tau^{(n)}(\mathbf{R}) = a\}$. ($\Gamma_\tau^{(n)}$ is also called the a-level curves which are a set of points $\mathbf{R} \in R^N$ for which the value of $\tau^{(n)}$ is a.) The propagation of these wave fronts depends on the "speed" function values on the wave front. The "slowness" function is similarly defined as $[2(E - V)]^n$. Solving Eq. 11 by a ray-based FMM we obtain the least-$\tau^{(n)}$ value for every conceivable configurations of the molecular system. From the least-$\tau^{(n)}$ value we determine the paths knowing that the vector $\nabla\tau^{(n)}$ for points on the level curves of $\tau^{(n)}$ is perpendicular at that point [30]. The method for calculating the paths is called back-tracing and is described in later sections.

Equation 11 is a first-order partial differential equations of second degree; exact solution of this equation is usually impossible. The method of characteristics [31,32] and the finite difference methods [33–35] are two widely used methods for solving the HJ equation. The use of the method of characteristics followed by interpolation is a popular and robust method for solving HJ equation, this reduces the partial differential equation to a set of ordinary differential equation (for instance, Hamilton's equations), the characteristic curves of which can cross depending on the potential. Thus, when the value of $\tau^{(n)}$ between a given source point ($\mathbf{R}_0$) and any other point (**R**) in the configuration space is sought, the method of characteristics delivers multiple values (weak solutions). In cases where actions on a grid of points are required, the interpolation of the ray-traced actions is essential, which makes the method even more complicated and time-consuming. The finite difference method on the other hand, attempts to track the wavefronts rather than the rays. A major advantage of this method is that the data are directly calculated on a grid of points, so no subsequent interpolation is required and the function is constrained to be single valued [33]. However, finite difference approximations to this type of hyperbolic partial differential equations may develop

singularities or shocks as they propagate, even if the initial wavefront is smooth. Osher and Sethian [30] noted that these shocks were avoided if one took the "viscosity solution" [36] to the Eq. 10; this led them to develop the level set method (LSM). The fast-marching method (FMM) of Sethian [12,13] adapts the LSM technique to compute the least arrival time by solving the eikonal equation. However, LSM and the FMM are based on a first-order finite-difference formula for the derivative on a Cartesian grid. In order to apply their FMM to molecular problems it is necessary to devise a different FMM which is applicable to any coordinate system. This is discussed in the next section.

3 Numerical evaluation of the least-$\tau^{(n)}$ surface and the reaction paths

3.1 Ray-based Fast marching method for a general coordinate system: finding least-$\tau^{(n)}$ surface

The Fast marching method is a minimization scheme which numerically solves the eikonal equation $1/F|\nabla U| = 1$ for the minimum value of U($\mathbf{Q}$) at point $\mathbf{Q}$. This is a minimization technique because it models only the wave that originates at the initial point, $\mathbf{Q}_0$, and terminates at $\mathbf{Q}$ and minimizes U; waves arriving at $\mathbf{Q}$ with larger values of U are totally filtered out. The fast marching method was originally proposed by Sethian and has been applied to solve numerous scientific problems e.g., image processing, computer vision, fluid mechanics, obstacle navigation, path planning, and moving interfaces. Here we adapt the method to solve the HJ equation (Eq. 11) in a general coordinate systems; in particular, we describe a ray-based updating algorithm below.

The method is described for a two-dimensional system. Extension to many-dimensional system is straightforward. The initial reactant configuration is defined as $\mathbf{R}_0 = (R_1^0, R_2^0)$. A compact wave is generated at the reactant configuration and then expands to engulf the entire classically-allowed region of the reacting system. Without any loss of generality, we can always consider the initial point to have $\tau^{(n)}(\mathbf{R}_0) = 0$.

For numerical purpose this system is defined in the rectangular domain $(R_1^{min}, R_1^{max}) \times (R_2^{min}, R_2^{max})$, which is partitioned into $N_{R_1} \times N_{R_2}$ cells of uniform size $\Delta R_1 \times \Delta R_2$ with their vertices $R_{ij} = (R_{1_i}, R_{2_j}) = (R_1^{min} + i\Delta R_1, R_2^{min} + j\Delta R_2)$. We now briefly describe the algorithmic steps associated with the fast marching method with emphasis on the ray-based updating procedure.

First, tag the point corresponding to the initial reactant $\mathbf{R}_0$ as *alive*, where $\tau_{i_0 j_0}^{(n)}$ is zero ((i_0, j_0) refers to the reactant state in the discrete grid). Then compute $\tau^{(n)}$ at all eight neighboring points ($(i_0 \pm 1, j_0 \pm 1)$, $(i_0, j_0 \pm 1)$, and $(i_0 \pm 1, j_0)$) in the first narrow band; these points are tagged as *close*. The remaining grid points are tagged as *far* and assigned $\tau^{(n)} - > \infty$. The FMM loop is carried out as follows.

Step a: Choose the point in *close* that has the smallest $\tau^{(n)}$ (this involves sorting the *close* points of the narrow band). Call this point *trial*. Remove *trial* from *close* points and add it to *alive*.
Step b: Tag as *close* all neighbors of *trial* that are not *alive*. (If the neighbor is in *far*, remove it from that set and add it to the set *close*).

Step c: Recompute $\tau^{(n)}$ at all the *close* neighbors of *trial*. This stage is called updating, and it is performed using the new technique described below.
Step d: If there are no more *close* points or if a stopping criterion is achieved, then the precedure is complete. Otherwise, go to step a.

Figure 1 presents a schematic view of the FMM algorithm describing how the *close* points in the narrow band become *alive* points and how the narrow band changes from the one at the initialization stage. Note that the leading term in the computational cost

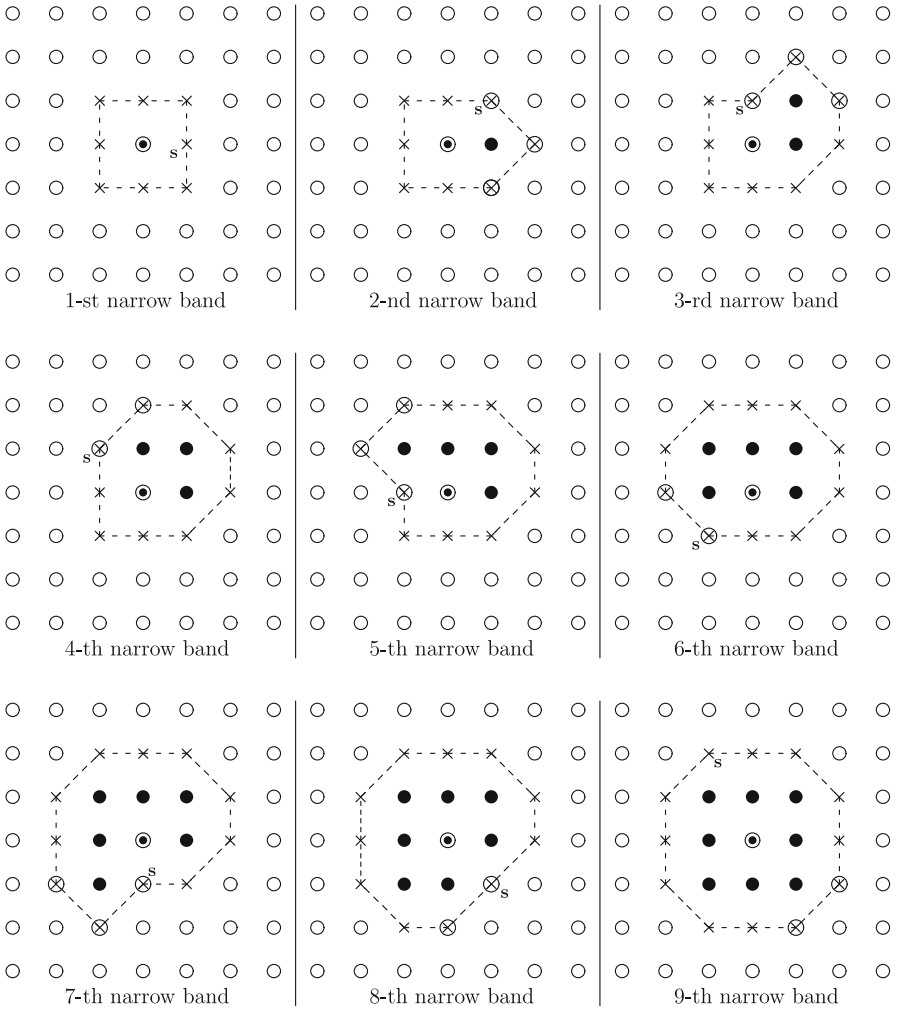

Fig. 1 Schematic diagram depicting different grid points for the narrow band. The narrow bands are obtained during the fast marching loop. The 1-st narrow band (first column, first row) is the one obtained at the initializing stage. Here the grid points with open circle, cross, cross in the circle, black dot and black dot in the circle represent *far*, *close* with no updating of the function value, *close* where function value will be updated, *alive* and initial (reactant) points respectively. Label s refers to the point wit smallest function value among the *close* points. Points on the broken line constitute the narrow band

of the fast marching algorithm comes from the step (a): that is, choosing the *trial* point on the narrow band with the smallest value of $\tau^{(n)}$. Consequently, the cost should not depend strongly on the updating stage, but rather the sort algorithm used. Heap sorting [37] has a cost of $O(logN)$, and so in principle, with the present algorithm, the fast marching method has a cost of $O(NlogN)$, where N is the total number of grid points.

3.2 Updating procedure

Now, we elaborate on the updating procedure needed for step (c) of the FMM loop. Let $\mathbf{R}^{(u)} = [R_1^{(u)}, R_2^{(u)}]^T$ be a *close* neighbor of the *trial* where the value of $\tau^{(n)}$ will be recomputed (updated). This point is represented by (i,j) in the 2D discrete grid. A four-point updating or an eight-point updating (or even more) can be done. The four-point updating uses the points $\mathbf{R}^{(1)} \equiv$ (i−1,j), $\mathbf{R}^{(2)} \equiv$ (i+1,j), $\mathbf{R}^{(3)} \equiv$ (i,j−1) and $\mathbf{R}^{(4)} \equiv$ (i,j+1) to update the value at (i,j), whereas the eight-point updating uses the points (see Fig. 2) $\mathbf{R}^{(1)} \equiv$ (i−1,j), $\mathbf{R}^{(2)} \equiv$ (i−1,j−1), $\mathbf{R}^{(3)} \equiv$ (i,j−1), $\mathbf{R}^{(4)} \equiv$ (i+1,j−1), $\mathbf{R}^{(5)} \equiv$ (i+1,j), $\mathbf{R}^{(6)} \equiv$ (i+1,j+1), $\mathbf{R}^{(7)} \equiv$ (i,j+1) and $\mathbf{R}^{(8)} \equiv$ (i−1,j+1). In the original FMM of sethian [12] only a four-point updating is implemented. The present algorithm is applicable to updating using any number of neighboring points and is also applicable to structured or unstructured mesh and to any type of coordinate systems. Here we discuss the 8-point updating procedure only. Updating based on more than eight points can be done similarly.

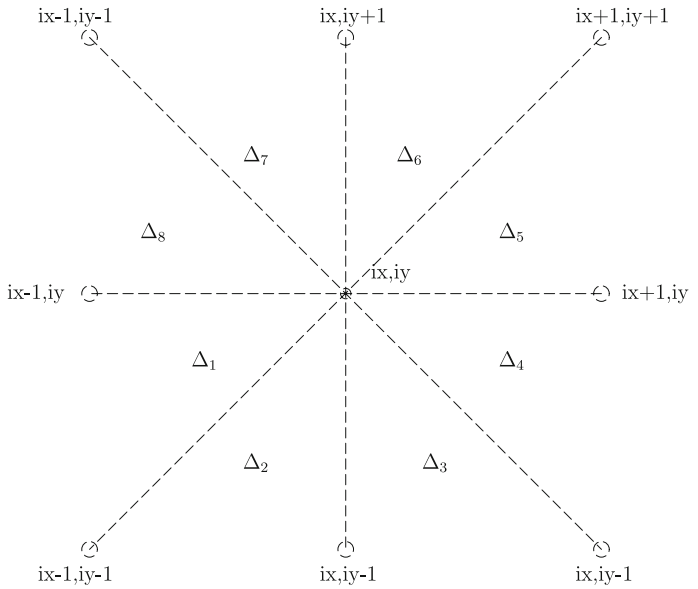

Fig. 2 Diagram depicting the triangles for a 8-point updating procedure. Point (ix,iy) is where the updated value of $\tau^{(n)}$ is computed. Only the upwind points (and hence the corresponding triangles) are required for updating

1. Designate eight triangles (see Fig. 2) formed by the eight points as $\Delta_1 = \Delta_{\mathbf{R}^{(1)},\mathbf{R}^{(2)},\mathbf{R}^{(u)}}$, $\Delta_2 = \Delta_{\mathbf{R}^{(2)},\mathbf{R}^{(3)},\mathbf{R}^{(u)}}$, $\Delta_3 = \Delta_{\mathbf{R}^{(3)},\mathbf{R}^{(4)},\mathbf{R}^{(u)}}$, $\Delta_4 = \Delta_{\mathbf{R}^{(4)},\mathbf{R}^{(5)},\mathbf{R}^{(u)}}$, $\Delta_5 = \Delta_{\mathbf{R}^{(5)},\mathbf{R}^{(6)},\mathbf{R}^{(u)}}$, $\Delta_6 = \Delta_{\mathbf{R}^{(6)},\mathbf{R}^{(7)},\mathbf{R}^{(u)}}$, $\Delta_7 = \Delta_{\mathbf{R}^{(7)},\mathbf{R}^{(8)},\mathbf{R}^{(u)}}$ and $\Delta_8 = \Delta_{\mathbf{R}^{(8)},\mathbf{R}^{(1)},\mathbf{R}^{(u)}}$. Here $\Delta_{a,b,u}$ represents a triangle formed by the grid line segments connecting the points a, b and u with u being the point where the $\tau^{(n)}$ will be computed.

2. The updated value of $\tau^{(n)}$ at $\mathbf{R}^{(u)}$ is given by

$$\tau^{(n)}_{updated}(\mathbf{R}^{(u)}) = min(\tau^{(n)}_{\Delta_1}, \tau^{(n)}_{\Delta_2}, \tau^{(n)}_{\Delta_3}, \tau^{(n)}_{\Delta_4}, \tau^{(n)}_{\Delta_5}, \tau^{(n)}_{\Delta_6}, \tau^{(n)}_{\Delta_7}, \tau^{(n)}_{\Delta_8})$$

   where $\tau^{(n)}_{\Delta_i}$ is the smallest solution of the ray-based procedure applied to the triangle, Δ_i.

3. We note that not all of the eight triangles will always contribute to the above equation since causality implies that points with values of $\tau^{(n)}$ that are larger than the point in question do not contribute. This causality requirement is the essence of the upwind derivative scheme.

3.3 Ray-based updating procedure from the triangle, $\Delta_{a,b,u}$:

Figure 3 depicts a wave front emanating from the source (the initial point, $\mathbf{R}^{(0)}$) and arriving at the point that is being updated (u). We need to find the minimum value of $\tau^{(n)}$ at the point, u, using the known values of $\tau^{(n)}$ at points a and b. $\mathbf{R}^{(u)}$, $\mathbf{R}^{(a)}$ and $\mathbf{R}^{(b)}$ are the position vectors for points u, a and b respectively, in the general coordinate system. The corresponding position vectors in the orthogonal co-ordinate system are $\mathbf{Q}^{(u)}$, $\mathbf{Q}^{(a)}$ and $\mathbf{Q}^{(b)}$ which are obtained as $\mathbf{Q} = \mathbf{P}^T\mathbf{R}$ where the matrix $\mathbf{P}$ diagonalizes the matrix $\mathbf{G}$ of Eq. 10, that is, $\mathbf{G} = \mathbf{PHP}^T$. We assume the wave front emanates from the source, passes through the line segment, a–b, (Fig. 3) and arrives at the point, u, so that the value of $\tau^{(n)}$ at u is minimum.

We now suppose that the wave front while reaching the point u intersects the a–b line segment at the transit point, t. The position vector of the transit point is $\mathbf{Q}^{(t)}$ (see Fig. 3). The function value at the various positions are $\tau^{(n)}_a$, $\tau^{(n)}_b$, $\tau^{(n)}_t$ and $\tau^{(n)}_u$ among which only $\tau^{(n)}_a$ and $\tau^{(n)}_b$ are known. The position vector, $\mathbf{Q}^{(t)}$, can be parameterized with the parameter $0 \leq \zeta \leq 1$ so that for $\zeta = 0$, $\mathbf{Q}^{(t)} = \mathbf{Q}^{(a)}$ and for $\zeta = 1$, $\mathbf{Q}^{(t)} = \mathbf{Q}^{(b)}$. This gives

$$\mathbf{Q}^{(t)} = (1-\zeta)\mathbf{Q}^{(a)} + \zeta\mathbf{Q}^{(b)} \tag{12}$$

The function value at the point, $\mathbf{Q}^{(t)}$, is now approximated by a linear interpolation formula

$$\tau^{(n)}_t = (1-\zeta)\tau^{(n)}_a + \zeta\tau^{(n)}_b. \tag{13}$$

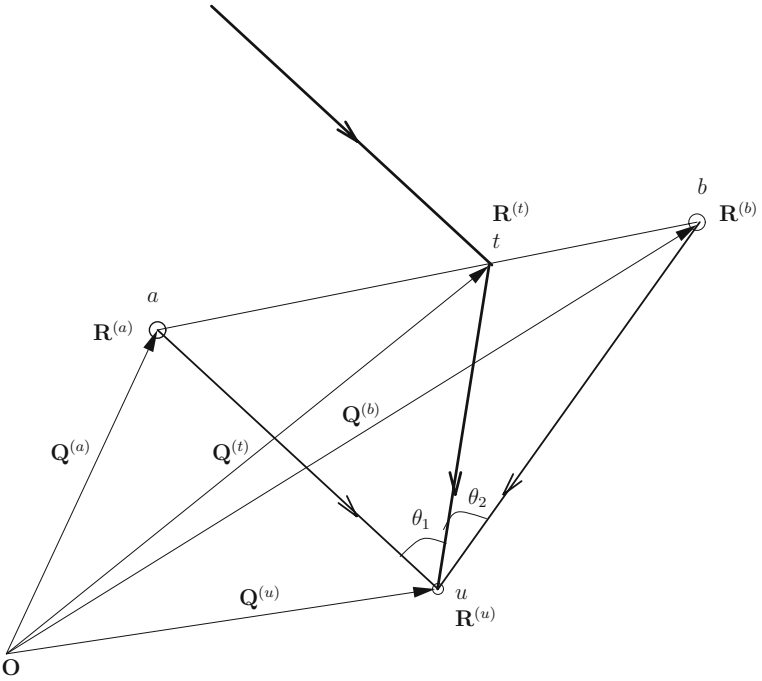

Fig. 3 Schematic diagram depicting the wave front reaching the point, u , where $\tau^{(n)}$ needs to be computed variationally. $\tau^{(n)}$ at the points a and b are known. The thick vector line shows the direction of the wave front from the source (not shown) to the point, u. Here t is the transition point that the wave front transits through to reach the point, u. Position vectors in the general coordinate systems, are $\mathbf{R}^{(u)}$, $\mathbf{R}^{(a)}$, $\mathbf{R}^{(b)}$ and $\mathbf{R}^{(t)}$ for the points u, a, b and t. O refers to the origin in the transformed coordinate system, where $\mathbf{Q}^{(u)}$, $\mathbf{Q}^{(a)}$, $\mathbf{Q}^{(b)}$ and $\mathbf{Q}^{(t)}$ are the position vectors in the transformed coordinate system for the points u, a, b and t. θ_1 and θ_2 are the angles of incidence that the direction vector of the wave front make with two sides of the triangle, $\Delta_{u,a,b}$

Now we need to find what extra $\tau^{(n)}$ is gained when the wave front travels along the line segment t–u. If v is the "speed" function for the wave front then the front travels a distance of v for unit change in $\tau^{(n)}$. So the extra gain in $\tau^{(n)}$ is $d(\zeta)/v = \sigma d(\zeta)$, where $d(\zeta)$ is the Euclidean distance between $\mathbf{Q}^{(t)}$ and $\mathbf{Q}^{(u)}$ and $\sigma = 1/v$ is the "slowness function. So, $\tau^{(n)}$ at $\mathbf{Q}^{(u)}$ is given by

$$\tau_u^{(n)} = \tau_t^{(n)} + \sigma d(\zeta) = (1-\zeta)\tau_a^{(n)} + \zeta\tau_b^{(n)} + \sigma d(\zeta) \tag{14}$$

According to the minimum-$\tau^{(n)}$ principle (e.g., minimum action, minimum time or minimum potential), the actual path is the path of minimum $\tau^{(n)}$ with respect to the perturbations of the wave front at $\mathbf{Q}^{(t)}$. Since the wave front at $\mathbf{Q}^{(t)}$ is parameterized with respect to ζ, we minimize $\tau^{(n)}$ by solving $\partial\tau_u^{(n)}/\partial\zeta = 0$, where $\tau_u^{(n)}$ is given by Eq. 14. The optimal value for ζ is obtained by solving the equation

$$\frac{\tau_a^{(n)} - \tau_b^{(n)}}{\sigma} = d'(\zeta). \tag{15}$$

The functions $d(\zeta)$ and $d'(\zeta)$ are given as

$$d(\zeta) = \sqrt{d_{ua}^2 + \zeta^2 d_{ba}^2 - 2\zeta(\mathbf{Q}^{(u)} - \mathbf{Q}^{(a)}) \cdot (\mathbf{Q}^{(b)} - \mathbf{Q}^{(a)})} \tag{16}$$

and

$$d'(\zeta) = \frac{\zeta d_{ba}^2 - (\mathbf{Q}^{(u)} - \mathbf{Q}^{(a)}) \cdot (\mathbf{Q}^{(b)} - \mathbf{Q}^{(a)})}{d(\zeta)} \tag{17}$$

respectively, where d_{ba} and d_{ua} are the Euclidean distances $|ba|$ and $|ua|$. Substituting $d'(\zeta)$ into Eq. 15 we get a quadratic equation for the unknown ζ whose solutions are

$$\zeta_{\pm} = \frac{\eta}{d_{ba}^2} \pm \sqrt{\frac{\eta^2}{d_{ba}^4} - \frac{\eta^2 - d_{ua}^2\left(\frac{\tau_a^{(n)} - \tau_b^{(n)}}{\sigma}\right)^2}{d_{ba}^2\left(d_{ba}^2 - \left(\frac{\tau_a^{(n)} - \tau_b^{(n)}}{\sigma}\right)^2\right)}} \tag{18}$$

where $\eta = (\mathbf{Q}^{(u)} - \mathbf{Q}^{(a)}) \cdot (\mathbf{Q}^{(b)} - \mathbf{Q}^{(a)})$. The value of ζ must be between 0 and 1. The updated value at the point, u, depends on the following different situations for the ζ.

1. If the term under the square root of Eq. 18 is negative then we do not evaluate the $\zeta_{\pm}$. In such a case, the updated value at the point, u, is given by

$$\tau_u^{(n)} = min(\tau_a^{(n)} + d_{ua} \times \sigma, \tau_b^{(n)} + d_{ub} \times \sigma) \tag{19}$$

   where $d_{ua} = |\mathbf{Q}^{(u)} - \mathbf{Q}^{(a)}|$ and $d_{ub} = |\mathbf{Q}^{(u)} - \mathbf{Q}^{(b)}|$ are the distances $|ua|$ and $|ub|$ in the transformed coordinate.

2. If only $0 \leq \zeta_+ \leq 1$, then we calculate

$$\tau_+^{(n)} = (1 - \zeta_+)\tau_a^{(n)} + \zeta_+ \tau_b^{(n)} \tag{20}$$

   Now we have to calculate $cos\theta_1$, and $cos\theta_2$ where θ_1 and θ_2 are the incident angles that the wave front makes with the two sides of the triangle $\Delta_{u,a,b}$ (see Fig. 3) where $cos\theta_1$ and $cos\theta_2$ are given by

$$cos\theta_1 = \frac{(\mathbf{Q}^{(a)} - \mathbf{Q}^{(u)}) \cdot (\mathbf{Q}^{(t)} - \mathbf{Q}^{(u)})}{|\mathbf{Q}^{(a)} - \mathbf{Q}^{(u)}||\mathbf{Q}^{(t)} - \mathbf{Q}^{(u)}|}$$

   and

$$cos\theta_2 = \frac{(\mathbf{Q}^{(t)} - \mathbf{Q}^{(u)}) \cdot (\mathbf{Q}^{(b)} - \mathbf{Q}^{(u)})}{|\mathbf{Q}^{(t)} - \mathbf{Q}^{(u)}||\mathbf{Q}^{(b)} - \mathbf{Q}^{(u)}|}$$

Here $\mathbf{Q}^{(t)} = (1-\zeta_+)\mathbf{Q}^{(a)} + \zeta_+\mathbf{Q}^{(b)}$. If $1/\sqrt{2} < cos\theta_1 < 1$ and $1/\sqrt{2} < cos\theta_2 < 1$ (for a 4-point updating scheme the conditions are $0 < cos\theta_1 < 1$ and $0 < cos\theta_2 < 1$), we take $\tau_+^{(n)}$ as the updated value, $\tau_u^{(n)}$ at the point u. Otherwise, updating will be done by using Eq. 19 in step 1.

3. If only $0 \leq \zeta_- \leq 1$, then we calculate

$$\tau_-^{(n)} = (1-\zeta_-)\tau_a^{(n)} + \zeta_-\tau_b^{(n)} \tag{21}$$

Similarly, now we have to calculate $cos\theta_1$, and $cos\theta_2$ for ζ_- as described above. If $1/\sqrt{2} < cos\theta_1 < 1$ and $1/\sqrt{2} < cos\theta_2 < 1$, then we take $\tau_-^{(n)}$ as the updated value, $\tau_u^{(n)}$ at the point u. Otherwise, updating will be done by using Eq. 19 in step 1.

4. If ζ_+ and ζ_- are both between 0 and 1 then we have to take the minimum of the updated values in step 2 and 3.

After the fast marching procedure is complete, we have a conical surface $\tau^{(n)}(\mathbf{Q})$, where the bottom of the cone is at $\tau^{(n)}(\mathbf{Q}_0) = 0$. For any molecular configuration of interest, $\mathbf{Q}$, the least $\tau^{(n)}$ path is simply the steepest descent path to $\mathbf{Q}_0$ starting at $\mathbf{Q}$. This path can be found by repeated steps in the direction $\nabla\tau^{(n)}(\mathbf{Q})/||\nabla\tau^{(n)}(\mathbf{Q})||$. The gradient can be evaluated using finite differences or radial interpolation [38,39], for example.

4 Illustration with $F+H_2$ and H+FH

Here we describe the calculation of the least-action ($\tau^{(1)}$)and least-time ($\tau^{(-1)}$) reaction paths for two collinear reaction systems, viz., $F + H_2 \rightarrow HF + H$ and HF+H→H+FH. These are the simplest reactions with curvilinear coordinate systems with the metric $\mathbf{G}$ given by

$$\mathbf{G} = \begin{pmatrix} \frac{1}{\mu_{H_2}} & -\frac{1}{2\mu_{H_2}} \\ -\frac{1}{2\mu_{H_2}} & \frac{1}{\mu_{HF}} \end{pmatrix} \quad and \quad \mathbf{G} = \begin{pmatrix} \frac{1}{\mu_{HF}} & -\frac{1}{2\mu_{F_2}} \\ -\frac{1}{2\mu_{F_2}} & \frac{1}{\mu_{HF}} \end{pmatrix} \tag{22}$$

for $F+H^aH^b$ and H^a+FH^b systems respectively. This system is specified by two coordinates R_1 and R_2 corresponding to the bond distances H^a–H^b (F–H^b for H+HF) and F–H^a (H^a–F for H+HF) respectively. The potential energy surface as a function of R_1 and R_2 is given by Stark et al. [40] in a many-body expansion form

$$V_{ABC}(\mathbf{R}) = \sum_i V_i^{(1)} + \sum_n V^{(2)}(R_n) + V_{ABC}^{(3)}(R_{AB}, R_{BC}, R_{AC}) \tag{23}$$

where $V_i^{(1)}$ (i = A,B,C) are the energies of the atoms, $V_n^{(2)}$ (n = AB, BC, AC) are the diatomic potentials of AB, BC and AC, and $V_{ABC}^{(3)}$ is a three-body potential, which

should become zero at all dissociation limits. In our examples, the index A refers to the F-atom (H-atom for H+HF), B to the H-atom (F-atom for H+HF) and C to the H-atom (H-atom for H+HF).

The diatomic potentials were expressed by extended Rydberg functions

$$V_n^{(2)} = -D_e(1 + a_1x + a_2x^2 + a_3x^3)e^{-a_1x} + a_4 \tag{24}$$

where D_e is the dissociation energy of the corresponding diatomic and x $= R_n - R_n^e$. The parameters a_4 is chosen so that $V_{ABC}(\mathbf{R})$ becomes zero at the asymptote. The three-body term $V_{ABC}^{(3)}$ was expressed [41] as a polynomial of order M,

$$V_{ABC}^{(3)}(R_{AB}, R_{BC}, R_{AC}) = \sum_{i,j,k}^{M} d_{ijk}\rho_{AB}^i\rho_{BC}^j\rho_{AC}^k, \tag{25}$$

with the constraints i+j+k≤M and i+j+k≠i≠j≠k. The variables ρ_n (n = AB,BC,AC) is given as

$$\rho_n = R_n e^{-\alpha_n(R_n - R_n^0)} \tag{26}$$

This potential was obtained by fitting the *ab initio* points on the potential energy surface calculated by the multireference configuration interaction method [42]. The parameters associated with the above potential are given by Stark et al. [40]. Table 1 lists the energy values for different configurations of the F+H_2 and H+FH systems.

Using this potential we solve the Hamilton-Jacobi equation (Eq. 11) for the least-action ($n = 1$) and the least-time ($n = -1$) following the fast marching technique described in Sect. 3. The starting point where the action/time is zero is considered as the reactant configuration near the entrance channel, $\mathbf{R}_0 = (1.4, 5.0)$ for F+H_2 and (1.74, 4.0) for H+FH (see Table 1). The product is the exit channel with **R** = (>2.0, 1.74) for both F+H_2 and H+FH reactions. Since in the FMM we obtain the least-action value for every discrete configurations, every point is a potentially important either as a product or intermediates. Hence in evaluating the path we consider varying final state configurations which are not necessarily the product configurations given in Table 1.

Table 1 Energy values for different configurations of the F+H_2 and H+FH

		E (kcal/mol)	R_1 (Bohr)	R_2 (Bohr)
F+H_2 reaction				
Reactant	F+H_2	-1.6×10^{-2}	1.4	5.0
Product	FH + H	−31.33	5.0	1.74
Saddle point	F–H–H	1.92	1.442	2.95
H+HF reaction				
Reactant	H+FH	−29.1	1.74	4.0
Product	HF+H	−29.1	4.0	1.74
Saddle point	H–F–H	9.77	2.125	2.125

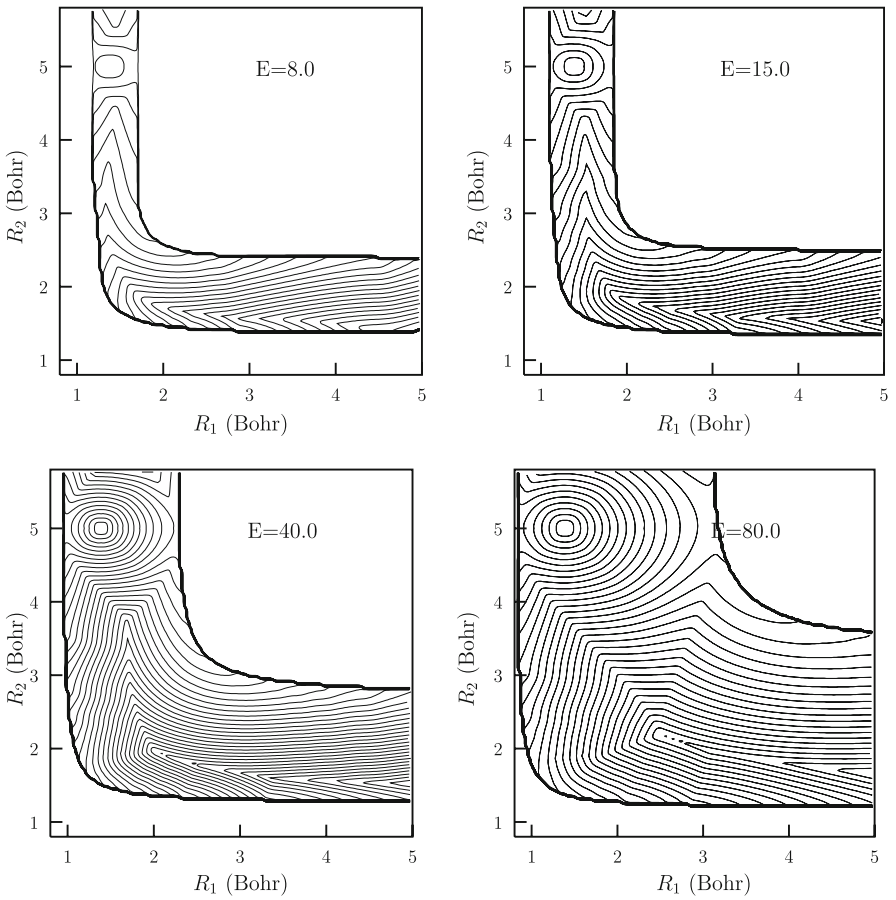

Fig. 4 Least-action ($\tau^{(1)}$) level curves of the collinear F+H_2 system at different energies (in kcal/mol) plotted as a function of $R_1 = R_{H_2}$ and $R_2 = R_{FH}$. The reactant (initial) state with S=0 is given by R_1=1.4 Bohr and $R_2 = 5.0$ Bohr

In the numerical calculation for the least-action (Fig. 4 for F+H_2 and Fig. 5 for H+FH) and least-time (Fig. 6 for F+H_2 and Fig. 7 for H+FH) level curves the grid size is $0.8 \leq R_1$ (Bohr) ≤ 5.0, $0.8 \leq R_2$ (Bohr) ≤ 6.5 for F+H_2 and $0.5 \leq R_1$ (Bohr) ≤ 5.0, $0.5 \leq R_2$ (Bohr) ≤ 1.0 for H+FH. We discretize each dimension into 150 small segments, thus we have a total of 150×150 discrete points. Each of these discrete points are a potential configuration of the reactive system. The least-action/least-time is calculated by fast marching method for all classically attainable configurations, that is, all configurations where $E > V_{ij}$. The FMM starts with initialization which consists of (1) defining an initial configuration, $\mathbf{R}_0 = (R_1^0, R_2^0)$ (which is the reactant configuration), (2) finding the associated indices (i_0, j_0) and setting the action/time values to be zero at this point, (3) defining the energy. The FMM procedure described in Sect. 3 is then commenced.

The least-action level curves in Figs. 4 and 5 show that the level curves extend to the regions of high potential as the energy values are increased. These figures reveal

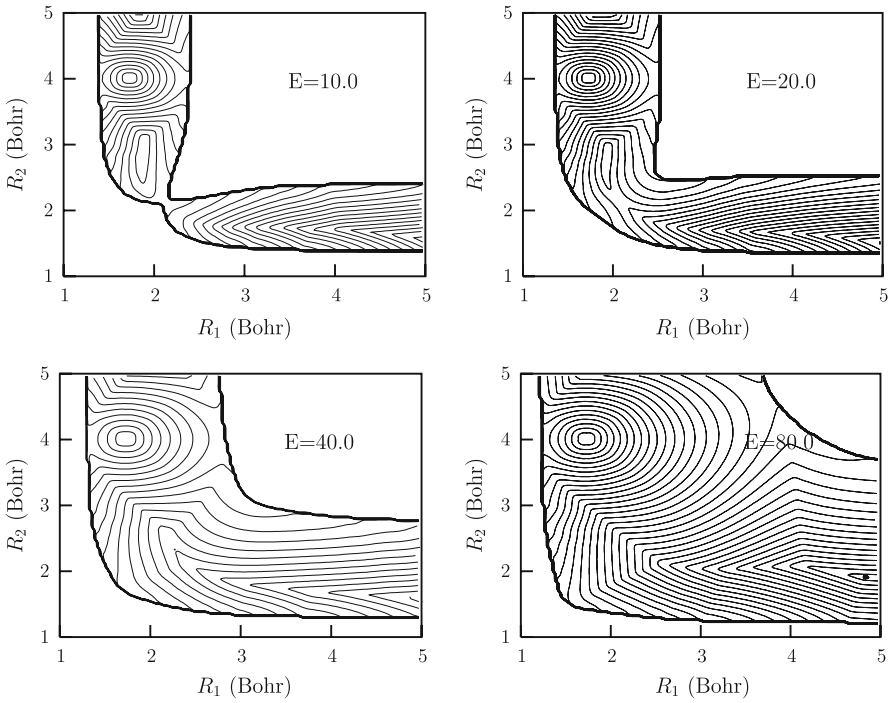

Fig. 5 Least-action ($\tau^{(1)}$) level curves of the collinear H^a+FH^b system at different energies (in kcal/mol) plotted as a function of $R_1 = R_{H^bF}$ and $R_2 = R_{H^aF}$. The reactant (initial) state with S=0 is given by $R_1 = 1.74$ Bohr and $R_2 = 4.0$ Bohr

the shape of the least-action wave fronts that emanate from $\mathbf{R}_0$ and spread over the classically attainable regions. The action values of the level curves increase with increasing distance from the initial configuration. Using the fact that the momentum vector $\mathbf{P} = \nabla\tau^{(1)}$, is normal to the surface of equal action and points in the same direction as the local unit normal $\nabla\tau^{(1)}/|\nabla\tau^{(1)}|$, we immediately get a pictorial representation of the reaction path for the reaction $\mathbf{R}_0 \longrightarrow R$ from Figs. 4 and 5. The presence of cusps on the least-action level curves seen in Figs. 4 and 5 as sharp corners makes it difficult to evaluate the gradient there. Such cusps develop at a least-action value where the potential, V is small (hence the kinetic energy is large) giving rise to $|\nabla\tau^{(1)}| \neq 0$. Since cusps develop in the low potential energy regions, numerical evaluation of low energy least-action path is difficult.

We also calculate the least-action paths for a high energy reaction E = 80 kcal/mol in Fig. 8. Several paths labeled a and b for the reaction F+H_2 and a,b,c for reaction H+FH are calculated and shown in Fig. 8 on the potential energy surface. These paths correspond to back-tracing from different product configurations, viz., (2.5, 2.4) (label a) and (2.6, 2.4) (label b) for F+H_2 reaction and (3.1, 2.1) (label a), (4.0, 2.1) (label b), (4.3, 2.1) (label c) for H+FH reaction. Since at the initial point, $\tau^{(1)}(\mathbf{R}_0) = 0$, may be thought of as shrinking a closed level curve to a single point, the construction of level curves around this point corresponds to considering every possible choice

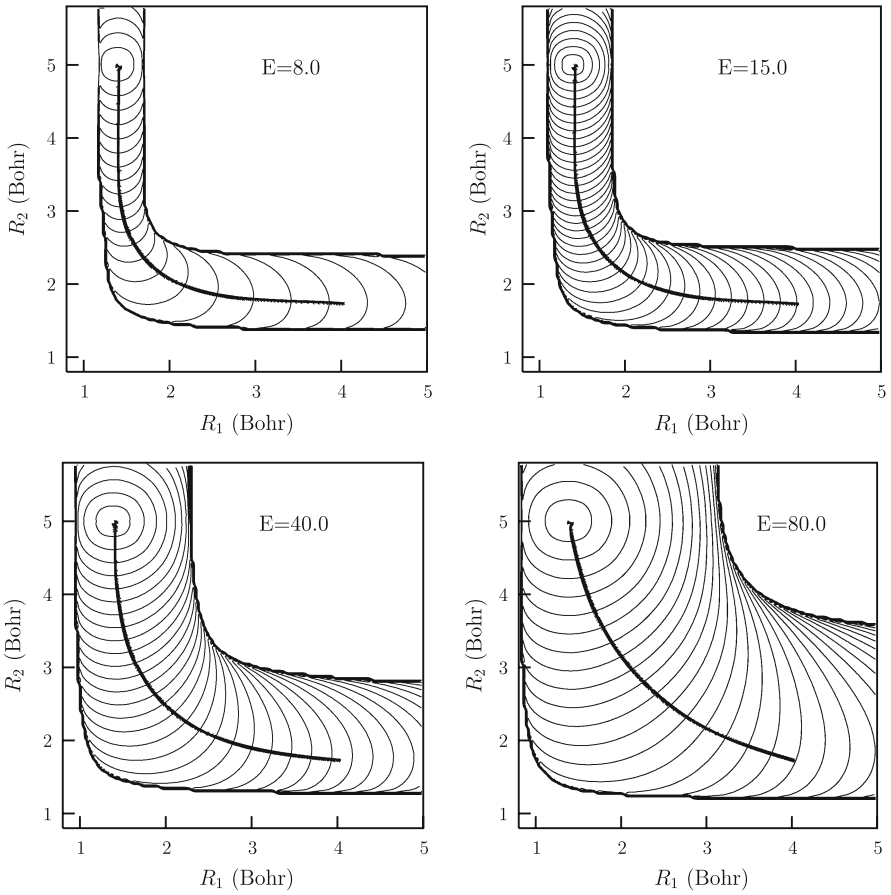

Fig. 6 Least-time ($\tau^{(-1)}$) level curves of the collinear F+H_2 system at different energies (in kcal/mol) plotted as a function of $R_1 = R_{H_2}$ and $R_2 = R_{FH}$. The reactant (initial) state with S=0 is given by $R_1 = 1.4$ Bohr and $R_2 = 5.0$ Bohr. Least-time paths are also shown. Only the path for E=8.0 goes over the saddle point, all other paths deviate from the saddle point and passes over the higher energy regions of the potential energy surface (also see Fig. 9)

for the gradient $\nabla\tau^{(1)}(\mathbf{R})|_{\mathbf{R}=\mathbf{R}_0}$ (that is, the initial momenta) consistent with the total energy of the system. Fast marching method ensures that we find one of the "ideal" initial momentum, $\mathbf{P}_0$ for which the reaction $\mathbf{R}_0 \longrightarrow \mathbf{R}$ occurs without the reactants spending much time (thus, the typical oscillations are removed) between the reactive event. The least-action paths shown in Fig. 8 for E=80 kcal/mol are reflective of this. We observe that the least-action paths for E=80 kcal/mol (label a for F+H_2 and a,b for H+FH) travel towards the classically-allowed high energy regions of the potential energy surface in order to form the product, the corresponding initial momenta for these paths can be obtained as $\nabla\tau^{(1)}(\mathbf{R})|_{\mathbf{R}=\mathbf{R}_0}$. This is in consistent with the discussions in Sect. 2.1.

The product configurations (2.6, 2.4) for the reaction F+H_2 cannot be traced back to the reactant configuration as seen in path labeled b. The back-traced paths from

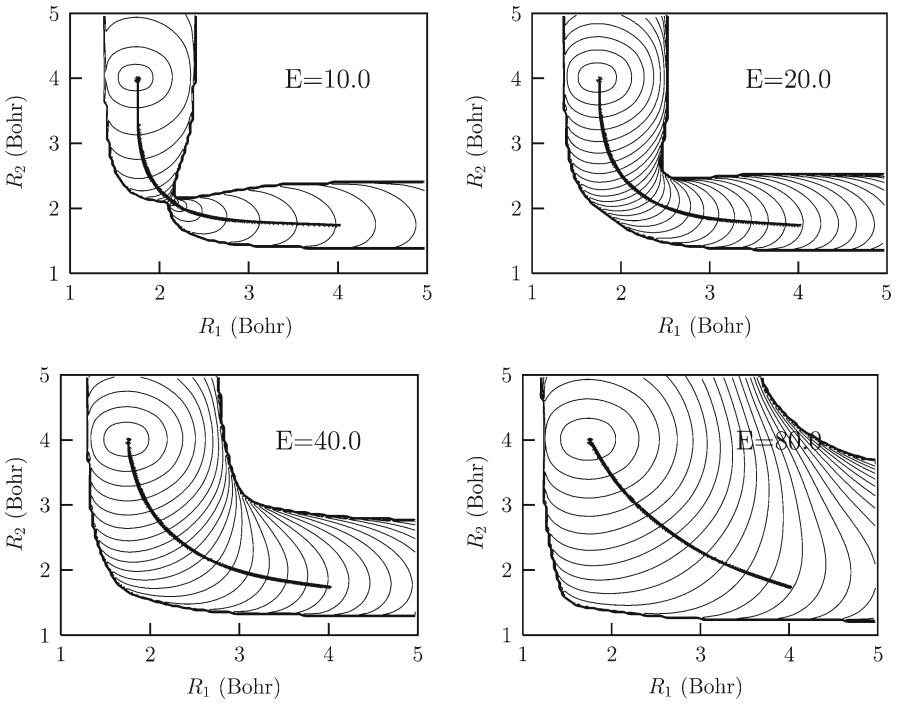

Fig. 7 Least-time ($\tau^{(-1)}$) level curves and the corresponding paths of the collinear H^a+FH^b system at different energies (in kcal/mol) plotted as a function of $R_1 = R_{H^bF}$ and $R_2 = R_{H^aF}$. The reactant (initial) state with S=0 is given by $R_1 = 1.74$ Bohr and $R_2 = 4.0$ Bohr. Only the path for E=10 goes over the saddle point. All other paths deviate from the saddle point and passes over the higher energy regions of the potential energy surface (also see Fig. 9)

these product states tend to cross the potential energy contours >80 kcal/mol (Fig. 8 upper panel) and hence they do not connect to the reactant states. Such paths and the corresponding products are dynamically insignificant and do not contribute to the dynamic properties of the reaction. Similarly, for the reaction H+FH the path c and the corresponding product is dynamically irrelevant. As has been discussed in Sect. 2.1, the high-energy least-time paths of Fig. 8 represent less probable dynamical events even though they correspond to one of the stationary action paths. Such paths are not kinetically relevant since they follow high-energy regions and are not associated with any of the transition states. Low-energy least-action paths, although difficult to calculate since $\nabla\tau^{(1)}$ is undefined at the cusps, are however, dynamically important events and can only be understood pictorially.

The least-time ($\tau^{(-1)}$) surface however, is devoid of cusps since $\nabla\tau^{(-1)}$ is related to $1/\sqrt{E-V}$. This is seen in Figs. 6 and 7 which depict the least-time level curves for F+H_2 and H+FH reactions respectively. The time value is zero at the reactant configuration (Table 1 for reactant configuration) which increases with the distance. As the energy increases we see that the least-time level curves extend over high energy regions of the potential energy. The level curves are much smoother than the ones for the least-action. Being devoid of cusps, the gradient $\nabla\tau^{(-1)}$ is defined at every

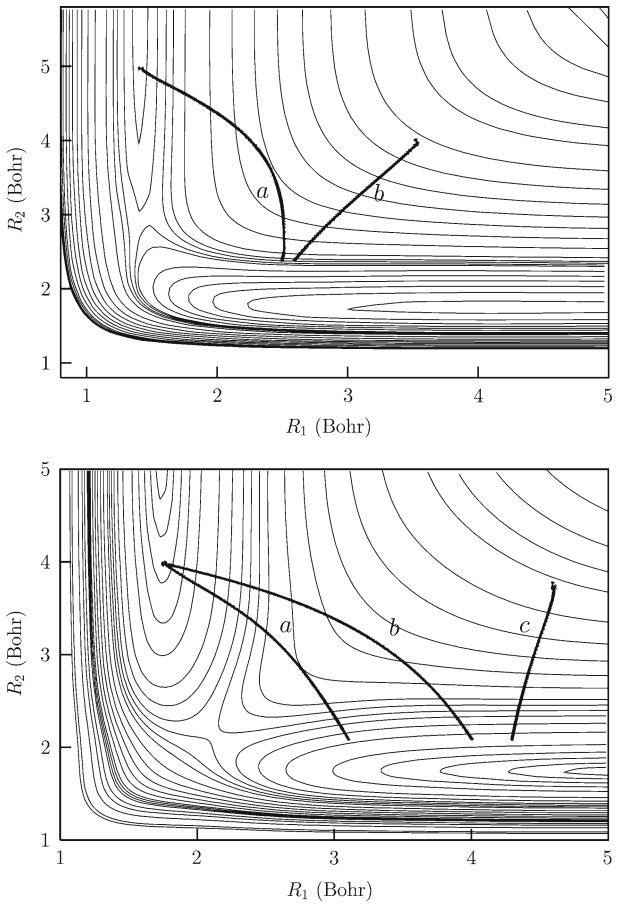

Fig. 8 Least-action ($\tau^{(1)}$) paths for F+H_2 (upper panel) and H+HF (lower panel) reactions calculated by back-tracing at E = 80 kcal/mol. The paths are shown on the potential energy surface. Labels a, b and c correspond to different paths

point on the level curves. This makes it easier to compute the paths following the back-tracing method. Indeed we can compute a large number of paths with one of the end point being the reactant state, however, we are interested in the paths that connect the reactant with a product state given in Table 1.

Reaction paths are shown on the least-time level curves of Figs. 6 and 7 for different energy values. The calculated least-time paths for the reaction event (1.4, 5.0) $\longrightarrow$ (4.0, 1.74) for the F+H_2 system and (1.74, 4.0) $\longrightarrow$ (4.0, 1.74) for H+FH system, traverse the low energy regions of the potential energy surface (also see Fig. 9 for the least-time paths plotted on the potential energy surface), unlike the least-action paths of Fig. 8. Some of the least-time paths cross the potential barrier near the saddle point (1.442, 2.95) for F+H_2 and (2.125, 2.125) for H+FH, in the PES to get to the product state. These are the paths calculated for low E. Such paths represent more probable dynamical events. Least-time paths plotted on the potential energy surface

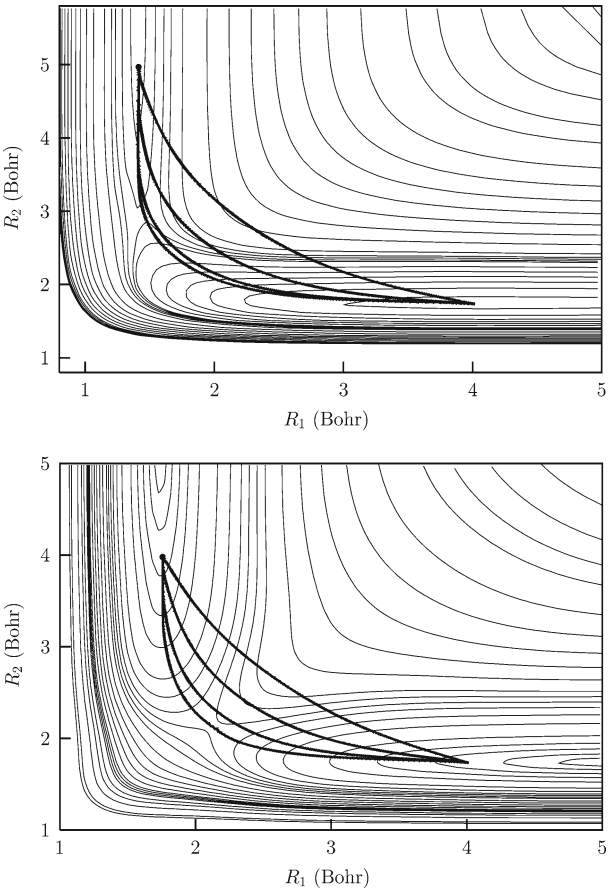

Fig. 9 Least-time ($\tau^{(-1)}$) paths for F+H_2 (upper panel) and H+HF (lower panel) reactions calculated by back-tracing at four different energy values shown in the respective least-time level curves of Figs. 6 and 7. The paths are shown on the potential energy surface. Low energy paths are very close to the saddle point whereas the higher energy ones deviate from the saddle point as energy increases

in Fig. 9 show that the barrier heights increase with increase in the energy for both the reactions. The barrier crossing at low energy takes place very close to the saddle point which however, starts deviating from the saddle point as energy increases. For example, data in Table 2 show that at E = 8 kcal/mol the barrier crossing for the reaction F+H_2 occurs at $(R_1^b, R_2^b) = (1.46, 2.93)$, while the saddle point lies at (1.442, 2.92). Similarly, for the reaction H+FH at E = 10 kcal/mol the barrier crossing takes place at $(R_1^b, R_2^b) = (2.126, 2.129)$ which is very close to the saddle point (2.125, 2.125). Table 2 gives information about the final configuration and the barrier configuration along the least-time path for different energy values. The time the path takes for the reactions F+$H_2 \longrightarrow$FH+H and H+FH$\longrightarrow$HF+H decreases as the energy increases, in other words, the reactions are faster for high energy. The barrier crossing times also decrease with increase in energy as is seen in Table 2.

Table 2 Datas at two different points (the final configuration (superscript f) and the barrier configuration (superscript b)) along the least-time paths

E(kcal/mol)	τ^f (fs)	τ^b (fs)	(R_1^b, R_2^b) (Bohr)
F+H_2 reaction			
8.0	1.016	0.537	(1.46, 2.93)
15.0	0.779	0.40	(1.53, 2.86)
40.0	0.506	0.264	(1.81, 2.75)
80.0	0.357	0.187	(2.18, 2.92)
H+FH reaction			
10.0	0.853	0.449	(2.126, 2.129)
20.0	0.495	0.249	(2.226, 2.224)
40.0	0.361	0.181	(2.39, 2.39)
80.0	0.257	0.128	(2.62, 2.62)

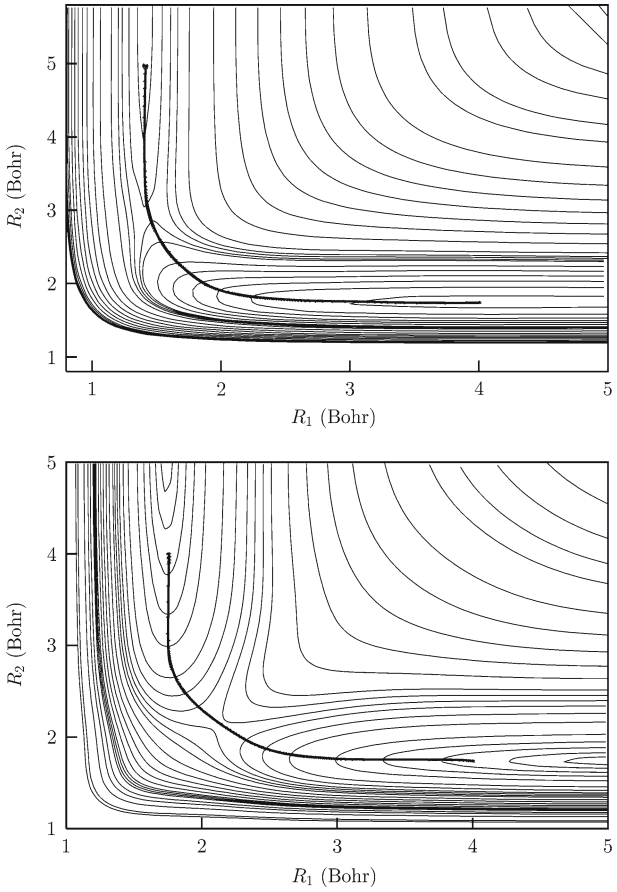

Fig. 10 Least-$\tau^{(-20)}$ paths for F+H_2 (upper panel) and H+HF (lower panel) reactions calculated by back-tracing for E = 80 kcal/mol. The paths are exactly the least-potential energy path. Least-time path for this energy follows the higher energy region (see Fig. 9)

Finally, we also have calculated the least-$\tau^{(-20)}$ path for both the reactions. These paths are shown in Fig. 10. As discussed in Sect. 2.1, the minimum energy path has no kinetic contribution and hence has no direct dynamical interpretation. This path is very close to the minimum energy path. Nevertheless, MEP has great theoretical and chemical importance. A uniquely defined and computable MEP forms the basis for the reaction rate theories. e.g., transition state theory (TST) or variational transition state theory (VTST). Typically, the MEP has the greatest statistical weight at any temperature, so the maxima on the MEP are the good candidates for the transition state (TS). From the knowledge of the MEP, the TST can give quite accurate estimates of the reaction rates.

5 Conclusion

In this paper, we have presented a new numerical method for solving the Hamilton-Jacobi equation in a general coordinate system. The method variationally determines the "fastest" ray that emanates from a fixed source point (taken as the reactant state configuration in our results) and arrives at any point in the configuration space. The minimum cost (that is, the minimum $\tau^{(n)}$) associated with these rays are also calculated variationally, which is then used to compute the reaction path. We have implemented this new method and showed some results for two reactive systems represented by a two-dimensional curvillinear coordinate system. The method provides a new way of predicting the products in any coordinate systems. The method differs from the traditional ones where the problem is posed as a initial value one ($\mathbf{R}_0$, P_0) or a boundary value one ($\mathbf{R}_0$, $\mathbf{R}_f$). This method does not require any optimization even though we are calculating the least-$\tau^{(n)}$ paths.

Extension of the method to include chemical dynamics in more complex molecular systems will require several computational developments. For example, a good interpolation scheme needs to be developed for evaluating the gradient from the known discrete values of the action/time; this is especially important for systems with many dimensions. The existence of the cusp in the least-action level curves and its behaviour must be throughly explored in order to construct a smooth least-action path. The approach has been tested with small systems where the potential energy surface is known analytically. It is clear this will not be the case in most chemical systems and one would need to evaluate the PES at every point picked by the fast marching machinery, preferably by using the available general purpose quantum mechanical codes. We are presently working in these direction, so that this approach will be useful in molecular dynamics involving larger molecular systems.

Acknowledgements The authors thank NSERC, McMaster University, the Canada Research Chairs, the Canada Foundation for Innovation, and the Ontario Innovation Trust for research support.

References

1. J.M. Haile, *Molecular Dynamics Simulation: Elementary Methods*. (Wiley, New York, 1992)
2. R. Car, M. Parrinello, Phys. Rev. Lett. **55**, 2471 (1985)
3. W.H. Miller, N.C. Handy, J.E. Adams, J. Chem. Phys. **72**, 99 (1980)

4. P.G. Bolhuis, C. Dellago, D. Chandler, Faraday Discuss. **110**, 421 (1998)
5. G. Henkelman, B.P. Uberuaga, H. Jonsson, J. Chem. Phys. **113**, 9901 (2000)
6. E. Elber, J. Meller, R. Olender, J. Phys. Chem. **B 103**, 899 (1999)
7. C. Jarzynski, Phys. Rev. **E 56**, 5018 (1997)
8. H. Grubmuller, Phys. Rev. **E 52**, 2893 (1995)
9. G. Henkelman, H. Jonsson, J. Chem. Phys. **111**, 7010 (1999)
10. B.K. Dey, M.R. Janicki, P.W. Ayers, J. Chem. Phys. **121**, 6667 (2004)
11. B.K. Dey, P.W. Ayers, Mol. Phys. **104**, 541 (2006)
12. J.A. Sethian, Proc. Natl. Acad. Sci. USA **93**, 1591 (1996)
13. J.A. Sethian, SIAM Rev. **41**, 199 (1999)
14. J.A. Sethian, *Level Set Methods and Fast Marching Methods*. (Cambridge Univ. Press, 1999)
15. B.K. Dey, S. Bothwell, P.W. Ayers, J. Math. Chem. (2006, in press)
16. B.K. Dey, P.W. Ayers, Mol. Phys. (2006, submitted)
17. T. Alkhalifah, S. Fomel, Geophys. Prospect. **49**, 165 (2001)
18. J.A. Sethian, V. Vladimirsky, PNAS **97**, 5699 (2000)
19. R. Kimmel, J. A. Sethian, Proc. Nat. Acad. Sci. **95**, 8341 (1998)
20. A.M. Popovici, J.A. Sethian, Geophysics **67**, 604 (2002)
21. J. Rickett, S. Fomel, Stanford Exploration Project Report **100**, 287 (1999)
22. Y. Sun, S. Fomel, Stanford Exploration Project Report **97**, 241 (1998)
23. H.K. Zhao, Math. Comput. **74**, 603 (2004)
24. C.Y. Kao, S. Osher, Y.H. Tsai, SIAM J. Numer. Anal. **42**, 2612 (2005)
25. W. Yourgrau, S. Mandelstam, *Variational Principles in Dynamics and Quantum Theory* (Sir Isaac Pitman and sons Ltd., Philadelphia, 1968)
26. E.T. Whittaker, *A Treatise on the Analytical Dynamics of Particles and Rigid Bodies* (Dover pub., New York, 1959)
27. W. Dittrich, M. Reuter, *Classical and Quantum Dynamics: from Classical Paths to Path Integrals* (Springer-Verlag, New York, 1992)
28. L.M. Landau, E.M. Lifshitz, *Classical Mechanics* (Butterworth-Heinenann, Oxford, 2000)
29. R. Courant, D. Hilbert, *Methods of Mathematical Physics*, vol II (Wiley, New York, 1989)
30. S. Osher, R. Fedkiw, *Level Set Methods and Dynamic Impicit Surfaces* (Springer, NY, 2003)
31. M. Spivak, *A Comprehensive Introduction to Differential Geometry*, vol 5, 2nd edn. (Perish Inc. Berkely, 1979)
32. V. Cerveny, J. Geophys. **58**, 2 (1985)
33. J.E. Vidale, Bull. Seis. Soc. Am. **78**, 2062 (1988)
34. J.V. Trier, W.W. Symes, Geophysics **56**, 812 (1995)
35. J.E. Vidale, Geophysics **55**, 521 (1990)
36. M.G. Crandall, H. Ishii, P.L. Lions, Bull. Am. Math. Soc. **27**, 1 (1992)
37. W.H. Press, S.A. Teukolsky, W.T. Vetterling, B.P. Flannery, *Numerical Recipes: the Art of Parallel Scientific Computing*, 2nd edn. (Cambridge Univ. Press, 1996)
38. M.J.D. Powel, in *Algorithm for Approximation of Functions and Data*, ed. by J.C. Malson, M.G. Cox (Oxford Univ. Press, 1987), pp. 143–167
39. M.D. Buhmann, Acta Numerica **9**, 1 (2000)
40. K. Stark, H.J. Werner, J. Chem. Phys. **104**, 6515 (1996)
41. A. Aguado, M. Paniagua, J. Chem. Phys. **96**, 1265 (1992)
42. M.J. Frisch, B. Lin, J.S. Binkley, H.F. Schaefer III, W.H. Miller, Chem. Phys. Lett. **114**, 1 (1985)